International Journal of Impact Engineering 113 (2018) 203–211

Contents lists available at ScienceDirect

International Journal of Impact Engineering

journal homepage: www.elsevier.com/locate/ijimpeng

The effect of curing agent on the dynamic tensile failure of an epoxy subjected to plate impact

Jonathan E. Pepper[a], Justin Huneault[b], Meysam Rahmat[c], Behnam Ashrafi[d], Oren E. Petel[*,a]

[a] Department of Mechanical and Aerospace Engineering, Carleton University, 1125 Colonel By Dr, Ottawa, ON, K1S 5B6, Canada
[b] Department of Mechanical Engineering, McGill University, 817 Sherbrooke St West, Montreal, QC, H3A 0C3, Canada
[c] Aerospace, National Research Council Canada, 1200 Montreal Rd, Ottawa, ON, K1A 0R6, Canada
[d] Aerospace, National Research Council Canada, 5145 Decelles Ave, Montreal, QC, H3T 2B2, Canada

ARTICLE INFO

Keywords:
Spall
Fracture toughness
Plate impact
Curing agent
Epoxy
PDV

ABSTRACT

Dynamic tensile failure of epoxy resin cured with two different curing agents was studied in terms of spall strength, fracture toughness, and shock behaviour. Plate impact experiments were conducted to examine how the epoxy responds to one-dimensional, high-strain rate loading. Velocity measurements of the back surface of the targets were taken during impact with a photonic-Doppler velocimeter (PDV). The velocity profiles that resulted were analyzed to gain insight on the material interface/stress wave interactions that manifested within the samples. Spall strength measurements ranged from 404 to 585 MPa in EPON 828 cured with EPIKURE 3223, and from 339 to 462 MPa in EPON 828 cured with EPIKURE 3233. Evidence for the existence of a quantifiable relationship between the curing agent used to cure the resin and the dynamic tensile strength of the resulting epoxy is provided. The discrepancies in the measured spall strengths between the two epoxy systems were attributed to a difference in the electrostatic forces between adjacent polymer chains within the crosslinked epoxy network. Strength measurements in both epoxies demonstrated significant strain-rate dependency. Spall strength measurements presented in this study were noticeably higher than those listed in the literature for similar thermosetting polymers, likely the result of the choice of curing agent. Finally, shock and particle velocity measurements were shown to be consistent with previously published results, within experimental uncertainty.

1. Introduction

Epoxy resins are thermosetting polymers that see widespread use in industry due to their favourable mechanical properties, which include high modulus and adhesion strength, low creep at elevated temperatures, and ease of application [1]. Epoxies are comprised of two parts: a resin and a curing agent. Mixing these two parts initiates a chemical reaction that yields a polymer with a highly-crosslinked network [2]. The kinetics of this reaction have a direct effect on the mechanical properties of the resulting epoxy, whereby variables such as cure temperature, mixing rate, stoichiometric ratio, and setting time all influence the polymerization process [2,3]. Developments in composite technology, such as the introduction of nanocrystalline materials into composite systems, have led to a resurgence in research relating to the dynamic characterization of epoxies [4–10]. Relevant applications include the use of epoxies as surrogate materials for polymeric binder phases in energetic materials [11,12], and as stand-ins for transparent armour [13–15].

Fully-integrated transparent armour is designed to resist ballistic assault without compromising structural integrity and optical transparency [13]. The strategies for selecting the appropriate materials for transparent armour systems depend primarily on the nature of the ballistic threats that will likely be encountered. Modern armour systems generally consist of three functional layers: (1) a hard strike face to blunt, fragment, and/or erode the projectile, (2) an intermediate layer with high energy-absorption and crack-arresting characteristics, and (3) a backing layer designed to arrest fragments and prevent outright penetration [13].

The penetration of armour is the result of competing effects from several dynamic material properties at appropriate strain rates and stress states, such as tensile strength, shear strength, compressive strength, hardness, and fracture toughness [14]. Knowing that microstructures influence these critical mechanical properties to varying extents, it is therefore possible to modify a microstructure in a stand-in material such as an epoxy to investigate how factors like cure-processing techniques, particle inclusion, and reaction kinetics affect the

* Corresponding author.
E-mail address: oren.petel@carleton.ca (O.E. Petel).

https://doi.org/10.1016/j.ijimpeng.2017.11.009
Received 21 June 2017; Received in revised form 18 October 2017; Accepted 15 November 2017
Available online 16 November 2017
0734-743X/ © 2017 Elsevier Ltd. All rights reserved.

aforementioned mechanical properties.

Early studies by Barker and Hollenbach [16] used plate impact experiments to study shock-wave propagation in polymethylmethacrylate (PMMA). They found that wave propagation was affected by the nonlinearity in the material, strain-rate dependence, and elastic-plastic effects. More recent experimentation by Jordan et al. [17] confirmed and expanded upon their findings. Carter and Marsh [18] conducted explosive shock-loading experiments on a selection of representative polymers. In addition to establishing their Hugoniot equations of state, they also observed a high-pressure transformation in all polymers characterized by a change in the slope of the U_s–u_p Hugoniot, and occasionally a large decrease in volume. They attributed these observations to shock-induced restructuring of the molecular backbone, where the transformation parameters were shown to be insensitive to the degree of crystallinity of the original bulk polymer. They also ruled out the possibility of the transformation being caused by melting or vaporization, since the behaviour was observed in both thermosetting and thermoplastic polymers.

Fu et al. [19] examined the shock response of polyethylene nanocomposites using a coarse-grained molecular dynamics simulation. Their analysis established a linear U_s–u_p Hugoniot relationship for the material within the range of tested particle velocities. They also found that nanoparticle modification generated an increase in Young's modulus and yield strength, especially for polymers with shorter backbone chains [19].

Chen et al. [20] used a modified split Hopkinson tension bar to study dynamic stress-strain responses and failure behaviour of PMMA and EPON 828/T-403 at strain rates on the order of $10^3\,s^{-1}$. They observed that the peak tensile strengths measured for EPON 828/T-403 under dynamic loading were achieved at smaller strains when compared to the quasi-static case. Furthermore, the specimens fractured in a brittle manner during dynamic tensile loading, while the quasi-static specimens failed in a ductile manner with a necking process, thereby providing qualitative evidence for a strain-rate effect. Plate impact experiments conducted by Curran et al. [21] were used to examine void nucleation and growth functions in polycarbonate by analyzing the incipient shock damage observed in recovered samples, while Faye et al. [22] investigated the mechanics of dynamic fracture of polycarbonate relative to that of PMMA using combined numerical and experimental approaches.

Millett et al. [23] conducted a thorough investigation into the effects of changing the chemistry of several polymers subjected to plate impact loading, where the electrostatic repulsion between adjacent polymer chains, as well as their molecular shape, were found to influence the shock response of the polymer. Millet et al. [24] also conducted plate impact experiments to study the behaviour of an epoxy resin under one-dimensional shock loading (impact velocities ranging from 201 to $833\,m\cdot s^{-1}$). By instrumenting the samples with longitudinal and lateral-oriented stress gauges, they were able to provide evidence for a shear strengthening effect similar to that observed in PMMA [25]. This result was attributed to the viscoelastic nature of epoxy resins.

Razack and Varghese [3] used thermogravimetric analysis (TGA), and differential scanning calorimetry (DSC) to investigate the effect of various hardeners (two aliphatic and two aromatic) on the properties of epoxy resin. Their results showed a clear divide in effectiveness between the thermal and mechanical performance of epoxy resin cured with aliphatic and aromatic hardeners, which is consistent with the work of Jain et al. [26] who studied curing kinetics and thermal stability in epoxy resins.

Munson and May [27] studied the high-pressure compressibility of EPON 828 resin cured with three curing agents. The equilibrium compression curves for the three epoxy systems were essentially identical at pressures above 1 GPa, whereas the quasi-static results showed significant variation between systems. This effect suggests that variation in structure and the degree of crosslinking between polymer chains has a negligible effect on high-pressure compressibility. Differences in the quasi-static compression curves were attributed to variation in the equilibrium distances and binding forces between adjacent polymer chains, which are determined by the choice of curing agent and degree of cure.

An investigation by Golubev et al. [28] showed that spall strengths of most amorphous polymers typically range between 100–300 MPa, where the observed spallation characteristics change with peak pressure. Samples recovered from plate impact experiments conducted at different temperatures showed zones of increasing plasticity near crack tips [28]. Despite observing a variety of fracture phenomena across a range of loading conditions, the spall strength of PMMA was shown to be invariant to increasing shock pressure [28] and only slightly sensitive to strain rate. Spall failure in epoxy has been studied by several researchers. Parhomenko and Utkin [29] published a spall strength of 300 ± 50 MPa for epoxy EDT-10 at an impact velocity of $850\,m\cdot s^{-1}$. Guess [30] reported a spall strength of 76 MPa for EPON 828 epoxy (strain-rate not specified) in his unpublished work.

While the dynamic tensile properties of these epoxy materials are well-documented, the effects of their various microstructural features on their performance under high-strain rate loading conditions is not as well understood. Specifically, the effect of the curing agent on the spall strengths of thermosetting polymers presents a knowledge gap in the literature, where one could expect to see an influence of the microstructure on macroscopic mechanical performance. This study seeks to fill this gap by providing insight into the effect of curing agents on the dynamic tensile properties of epoxy resin. Plate impact experiments were conducted to measure the spall strength of EPON 828 resin cured with two different curing agents. A discussion of the observed failure behaviour is also provided to supplement the results of this investigation.

2. Materials and methods

EPON 828 is an undiluted, clear, difunctional, bis-phenol A liquid epoxy resin with an epoxy equivalent weight (EEW) of $185–192\,g\cdot mol^{-1}$. The structure of the base EPON 828 resin molecule is shown in Fig. 1 [2]. The first curing agent used in this study was EPIKURE 3223, an unmodified aliphatic diethylenetriamine (DETA). The second curing agent was EPIKURE 3233, which is an unmodified aliphatic polyoxypropylenetriamine. A concise description of the physical meanings associated with the nomenclature of each compound is provided by Razack and Varghese [3]. All epoxy materials (curing agents and resin) were sourced from Hexion Inc. For clarity, the epoxy systems that resulted from curing EPON 828 resin with EPIKURE 3223 and EPIKURE 3233 will henceforth be referred to as EPON 828-A and EPON 828-B, respectively. The EPON 828-A specimens were prepared with a resin-to-curing agent mix ratio of 100:12 by weight. The EPON 828-B specimens were prepared with a resin-to-curing agent mix ratio of 100:43 by weight. All specimens were subjected to a post-cure procedure based on manufacturer recommendations [31–33].

Uniaxial tensile testing was conducted for both epoxy systems under quasi-static conditions. Five dogbone specimens of each epoxy were tested according to ISO 527-2 (Type 1BB), where samples with a gauge length 12.0 mm were loaded at an extension rate of $2\,mm\cdot min^{-1}$. Testing was performed at 21°C with a Fullam substage test frame. The

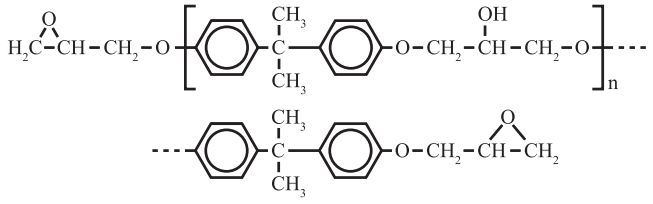

Fig. 1. The molecular structure of EPON 828 resin [2].

Table 1
The relevant physical properties of all materials used in the plate impact experiments.

Material	ρ_0 ($g \cdot cm^{-3}$)	C_0 ($km \cdot s^{-1}$)	C_L ($km \cdot s^{-1}$)	Z ($GPa \cdot s \cdot m^{-1}$)	σ_{max} (MPa)	ϵ_{max}	E (GPa)	K_c ($MPa \cdot m^{½}$)
6061-T6	2.700[a]	5.35[c]	6.40[c]	14.44	310[a]	0.120[a]	68.9[a]	29[a]
PMMA	1.193[b]	2.60[c]	2.72[c]	3.08	72.4[b]	0.050[b]	3.10[b]	1.55[d]
EPON 828-A	1.185[c]	2.64[c]	2.63[c]	3.13	65.0	0.046	2.65	1.02
EPON 828-B	1.185[c]	2.64[c]	2.63[c]	3.13	58.6	0.037	2.85	2.07

[a] Glemco Inc. [34]
[b] Arkema Inc. [35]
[c] Carter and Marsh [18]
[d] Weerasooriya et al. [36]

average of the maximum tensile strength (σ_{max}) measurements recorded for EPON 828-A and EPON 828-B are reported in Table 1 with associated standard deviations of 2.46 and 1.53 MPa, respectively. The average values of tensile strain at σ_{max} (ϵ_{max}) and Young's modulus (E) are also reported in Table 1.

Plane-strain fracture toughness (K_C) measurements were taken for both epoxy systems under quasi-static conditions. Five rectangular specimens (2 mm × 4 mm × 20 mm) for each epoxy were prepared in a Teflon mould. A precision saw was used to create a notch on the samples. The notch was then sharpened with a razor blade. Preparation of the notches and testing were conducted according to ASTM D 5945 at 21°C with a Fullam substage test frame. The extension rate was 3 $mm \cdot min^{-1}$. The average of the K_C measurements recorded for EPON 828-A and EPON 828-B are reported in Table 1 with associated standard deviations of 0.14 and 0.24 $MPa \cdot m^{½}$, respectively.

It is vital to note that the values of C_L and C_0 reported in Table 1 for EPON 828-A and EPON 828-B were not obtained from our own ultrasonic (pulse-echo transit) measurements, but rather, were taken directly from data for EPON 828 presented by Carter and Marsh [18]. These sound speeds will be assumed to be independent of the curing agent and valid for calculations of spall strength.

The epoxy samples used for the plate impact experiments were machined from cast plates that were subjected to a post-cure procedure. The surfaces of the EPON 828-A samples were not polished after machining (i.e., kept in their as-machined state), whereas the front and back surfaces of the EPON 828-B targets were polished with a stepwise process that used up to 400 grit sandpaper to remove any visible surface imperfections. The thicknesses of the targets (w_t) used in the experiments ranged between 5.38 and 8.45 mm.

Polymethylmethacrylate (Plexiglas® G) was also tested during this series of plate impact experiments. It is an amorphous thermoplastic more commonly referred to as acrylic or PMMA. It was used as a means of validating our techniques by comparing our results with data reported previously in the literature. The PMMA specimens for these plate impact spall experiments were machined to size from 9.53 mm sheet stock. Uniaxial tensile testing and plane-strain fracture toughness testing was not performed for PMMA under quasi-static loading conditions, since σ_{max} and K_c are quite well documented for this material [35,36].

A single-stage light gas gun with a smooth internal bore of 64 mm was used for this series of impact experiments. The gun generated projectile impact velocities (v_i) between 118 and 722 $m \cdot s^{-1}$. A schematic of the gun and the target assembly are shown in Figs. 2 and 3, respectively. The projectiles comprised of a plastic (nylon or PVC) sabot fitted with a flyer plate made from either 6061-T6 aluminum or PMMA. The aluminum and PMMA flyer plates (60 mm diameter) were laser cut from 1.96 mm and 1.55 mm thick sheet stock, respectively. A relief port was drilled through the wall of the sabot into an air gap located directly behind the flyer plate. The purpose of this relief port was to allow the gas pressure on both sides of the flyer plate to equilibrate during the evacuation of the catch tank, which helped eliminate any undesired flexing/loading of the flyer plate. Prior to launching the projectile, the

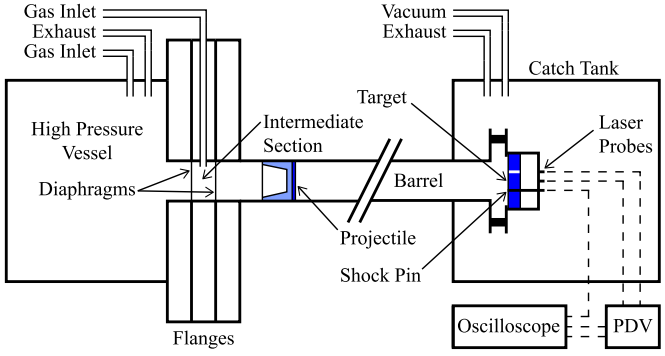

Fig. 2. A labeled schematic of the single-stage light gas gun.

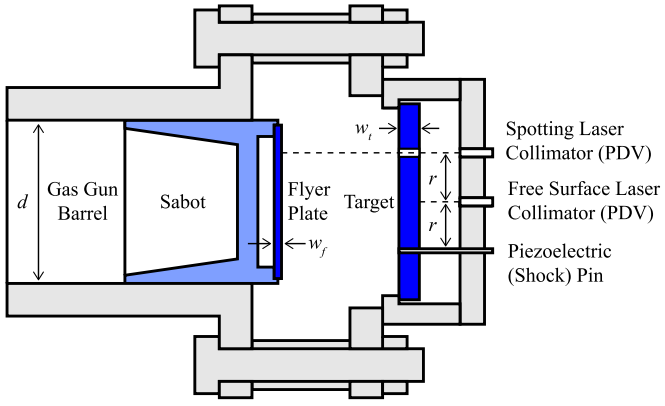

Fig. 3. A labeled schematic of the target assembly, where d = 64 mm, r = 25.4 mm, and w_f = 1.96 or 1.55 mm.

catch tank was evacuated to a pressure of approximately 150 Pa.

The impact and response of the test samples was investigated with a piezoelectric (shock) pin and a two-channel photonic-Doppler velocimeter (PDV) [16,37] represented schematically in Figs. 2 and 3. The shock pin was mounted flush with the front face of the target. The PDV system was used to measure the velocity of the flyer and the back surface of the target with separate collimators. The velocity history of the flyer plate was monitored by a spotting laser projected through a hole drilled through the target. The spotting laser was also used to provide an ancillary method of measuring the time of arrival (TOA) of the flyer plate. Our PDV system used a 1550 nm infrared laser, however EPON 828 epoxy and PMMA are not infrared-reflective, which made it impossible to take direct measurements of the free surface velocity during impact. It was therefore necessary to introduce a reflective buffer material to the back face of each sample. This was achieved by using a semicore inline sputtering system to coat the back surface with a 40–60 nm layer of aluminum. This process required the samples to be held in a vacuum chamber for several hours to allow for sufficient degassing of the material, followed by the coating process, which

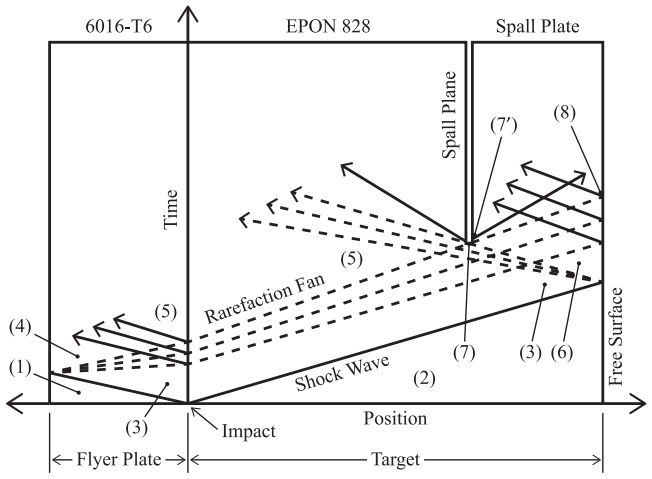

Fig. 4. A position-time plot depicting the wave interactions that occur during an asymmetrical plate impact ($Z_{Flyer} > Z_{Target}$). Dash lines represent rarefaction wavelets, while solid lines represent shock waves. Free surface and interface motion are not depicted.

occurred at a temperature of 50°C. It was found that the quality of the coating improved if the samples were polished prior to subjecting them to the sputtering system.

3. Theory

The primary wave interactions within the target for a spall test are illustrated in Fig. 4, where the relationship between the specific acoustic impedances (Z) of the flyer plate and target influence the nature of these wave interactions [38]. As seen in Figs. 4 and 5, the interactions of the rarefaction fans will result in the generation of a large tensile stress within the sample (state 7 in Fig. 5). If this tensile stress exceeds the local strength of the material, and partial or complete fracture is observed, then either incipient or total spall failure is said to have occurred [39–43]. The magnitude of the tensile stress that produces any degree of spall damage is designated as the spall strength of the target material [39,40]. Therefore, spall failure can be defined as dynamic tensile failure caused by the interaction of rarefaction waves within a material that are generated during high-strain rate deformation [41]. Spall strength is often used in combination with parameters such as fracture toughness, ballistic limit, energy absorption, and hardness to quantify resistance to dynamic failure caused by ballistic impact.

Given that spall failure is the result of wave interactions involving

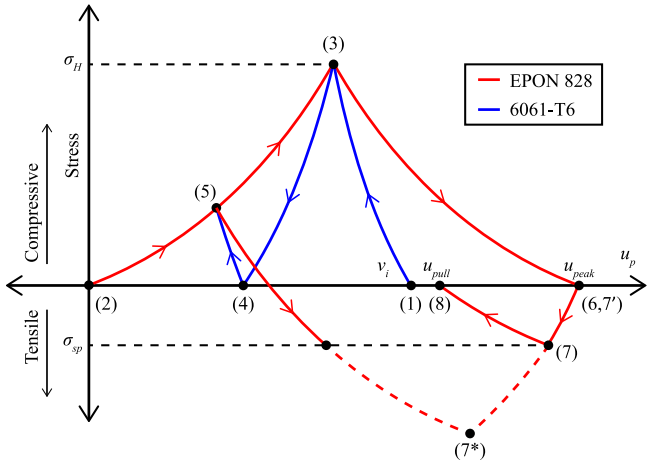

Fig. 5. A schematic of the stress-u_p plane associated with the impact shown in Fig. 4. States (1)–(8) are shown in both figures. The dashed line from (5) to (7*) represents the loading path followed by the target for a sub-critical impact [8].

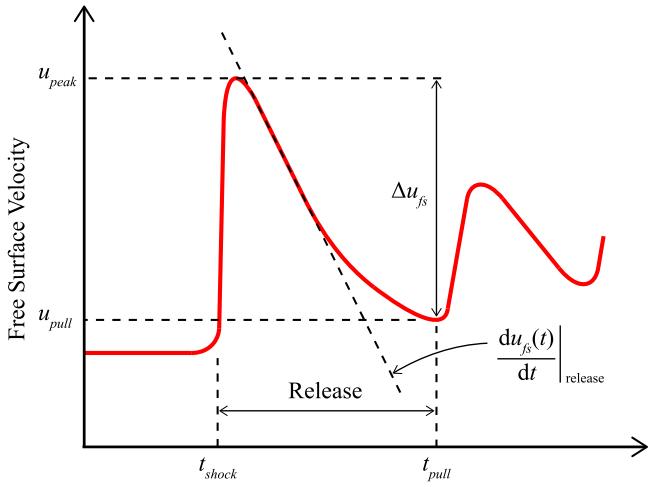

Fig. 6. A schematic plot of a free surface velocity profile obtained from a spall experiment.

significant material motion (see Fig. 5), the spall strength of a material is determined from the analysis of the velocity profile of the back (free) surface of the sample. The features of the velocity profile are directly representative of the interactions between the compressive shock waves, rarefaction fans, and target interfaces during impact [39,41]. A generic example of a free surface velocity profile is shown in Fig. 6, with the critical features labeled for reference. The post-shock particle velocity (u_p) is given by [38]

$$u_p \approx \frac{1}{2}u_{peak}. \tag{1}$$

Based on the wave interactions at the free surface, the velocity of the initial shock wave (U_s) that is transmitted through the target can be determined from the transit time of the wave through the sample. In the case of an attenuated (i.e., triangular) shock front, U_s more accurately describes the average velocity of the shock wave [38]. The experimentally-determined values of U_s and u_p were used to parameterize the constitutive shock Hugoniots for the two epoxy systems. For most materials these equations take the linear form [38]

$$U_s = C_0 + su_p, \tag{2}$$

where C_0 is the bulk sound speed and s is a non-dimensional parameter. Many polymers (such as PMMA) possess a distinctly non-linear $U_s - u_p$ relationship [16]. The Hugoniot state stress (σ_H) and corresponding volumetric strain (ϵ_H) achieved in the shock-compressed target are determined from the Rankine-Hugoniot equations [38,44,45]

$$\sigma_H = \rho_0 U_s u_p, \tag{3}$$

$$\epsilon_H = 1 - \frac{\rho_0}{\rho_H} = \frac{V_H - V_0}{V_0} = \frac{u_p}{U_s}, \tag{4}$$

where ρ_0 and V_0 are bulk density and volume, respectively, and ρ_H and V_H are density and volume in the shocked state, respectively. Note that it is necessary to assume steady wave propagation (all parts of the wave front travel at identical velocities) when using Eq. (3) and (4) to analyze viscoelastic materials such as epoxy [27]. The spall strength (σ_{sp}) of the target material can be predicted from the free surface velocity profile using an acoustics approach that gives the well-known linear approximation [39,43,46]

$$\sigma^*_{sp} = \frac{1}{2}\rho_0 C_L \Delta u_{fs}, \tag{5}$$

where the characteristic change in the free surface velocity (Δu_{fs}) is given by the difference between the observed peak velocity (u_{peak}) and pullback velocity (u_{pull}) (see Fig. 6)

$$\Delta u_{fs} = u_{peak} - u_{pull}. \tag{6}$$

An alternative relationship for spall strength was proposed by Stepanov [47], where

$$\sigma_{sp} = \rho_0 C_L \Delta u_{fs} \frac{1}{1 + \frac{C_L}{C_0}}. \tag{7}$$

This relationship, rather than Eq. (5), is used in the present study to calculate spall strength since it accounts for effects of elastic-plastic deformation in the sample [39]. The tensile strain rate achieved during the release stage is given by the expression [48]

$$\dot{\varepsilon}_r \approx \frac{1}{2C_0} \frac{\mathrm{d}u_{fs}(t)}{\mathrm{d}t}\bigg|_{\text{release}}, \tag{8}$$

where the $\frac{\mathrm{d}u_{fs}(t)}{\mathrm{d}t}$ term was defined in Fig. 6. The strain rate at which tension is applied to the test material is determined by the properties and thicknesses of the flyer plate and target materials. Using the magnitudes of σ_{sp} and $\dot{\varepsilon}_r$ it is possible to calculate the fracture toughness (K_c) of the target using the model proposed by Grady for brittle fracture [49] such that

$$K_c = \sqrt{\frac{\sigma_{sp}^3}{3\rho_0 C_0 \dot{\varepsilon}_r}}. \tag{9}$$

This model assumes that spall failure occurs in a brittle manner (i.e., through the lineup of a network of cracks to create an internal a free surface) [49]. It has been shown that epoxy demonstrates brittle fracture when loaded at elevated strain rates [50–52], which validates the use of Eq. (9) to determine K_c for the epoxy systems examined in the present study.

4. Results

An example of a binary waveform retrieved from the raw PDV data is shown in Fig. 7(a). The binary waveform is processed with a windowed Fourier transform that returns a spectrogram showing a distribution of laser beat frequencies, where the dominant frequency is associated with the motion of the target material [37,53]. The spectrogram that corresponds to the binary waveform presented in Fig. 7(a) is shown in Fig. 7(b).

The shock transit times were used to determine the shock Hugoniots of the test materials. The shock Hugoniot data for the two EPON 828 epoxy systems are plotted against data obtained by Carter and Marsh [18] (curing agent not specified) in Fig. 8. These results demonstrate that the shock Hugoniot is not particularly sensitive to the curing agent in this epoxy. The particle velocity was directly measured from the back face PDV signal and verified with an analytical impedance-matching technique [38] using the approach described by Petel and Higgins [54]. These two approaches were in close agreement, despite the presence of ejecta signals.

Three representative spectrograms are given in Figs. 9–11, which differ slightly as a result of the flyer plate used in the impact. Aside from the dominant signal, the spectrograms feature high-velocity horizontal signal bands at the free surface following shock arrival. These bands are reminiscent of PDV signals for ejecta plumes and are interpreted as ejecta from the sputtered aluminum coating on the target [55]. Reducing the surface roughness by polishing the EPON specimens lessened the severity of the ejecta plume.

There are two main types of results observed in the spectrogram images: a sub-critical (i.e., non-spall) impact and spall events. Fig. 7(b) is considered a non-spall event, identified by the oscillatory velocity profile and the absence of a characteristic spall (i.e., pullback) signal. Fig. 10 shows the spectrogram of a spall event in the same material, which exhibits all of the characteristics of the idealized signal shown in Fig. 6.

The experimental velocity profiles were analyzed to determine the

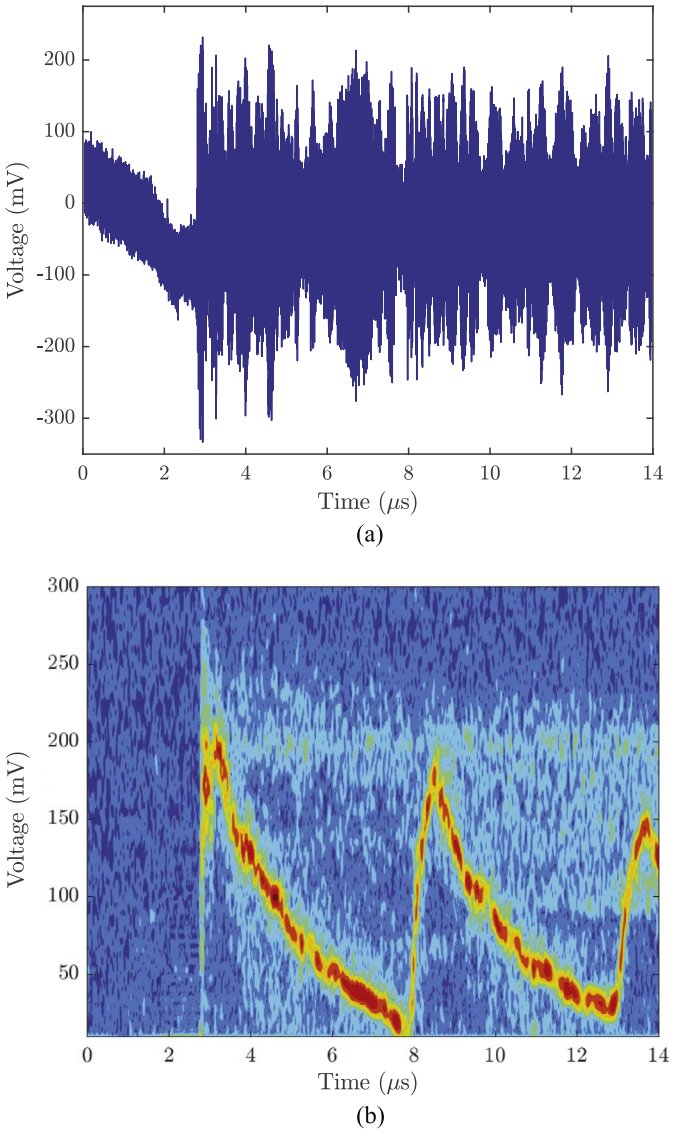

Fig. 7. (a) The waveform retrieved from the raw PDV signal of a polished EPON 828-B target impacted with a 6061-T6 aluminum flyer plate at a velocity of 118 $\mathrm{m \cdot s^{-1}}$. (b) The spectrogram of a non-spall event.

dynamic tensile properties of EPON 828-A, EPON 828-B, and PMMA. The spall strengths measured for PMMA ranged between 153 and 199 MPa for impact velocities between 203 and 722 $\mathrm{m \cdot s^{-1}}$. The fracture toughness of PMMA was found to range between 2.03 and 3.76 $\mathrm{MPa \cdot m^{1/2}}$ for strain rates on the order of 10^4 $\mathrm{s^{-1}}$. These values are consistent with spall strengths of 130 to 210 MPa [29] and fracture toughnesses of 2.5 to 4.1 $\mathrm{MPa \cdot m^{1/2}}$ [36] reported in the literature for PMMA at similar strain rates.

In the present study, the spall strengths for EPON 828-A and EPON 828-B were found to range from 404 to 585 MPa and from 339 to 397 MPa, respectively. The fracture toughness of EPON 828-A ranged between 14.8 and 19.0 $\mathrm{MPa \cdot m^{1/2}}$ for strain rates on the order of 10^4 $\mathrm{s^{-1}}$, whereas the values for EPON 828-B were slightly lower, ranging between 8.95 and 11.6 $\mathrm{MPa \cdot m^{1/2}}$. A summary of the experimental results are presented quantitatively in Table 2 and graphically in Figs. 12–15.

5. Discussion

The shock Hugoniot measurements from the present study (Fig. 8) are in agreement, within experimental uncertainty, with data reported previously for EPON 828 [18]. This implies that the choice of curing

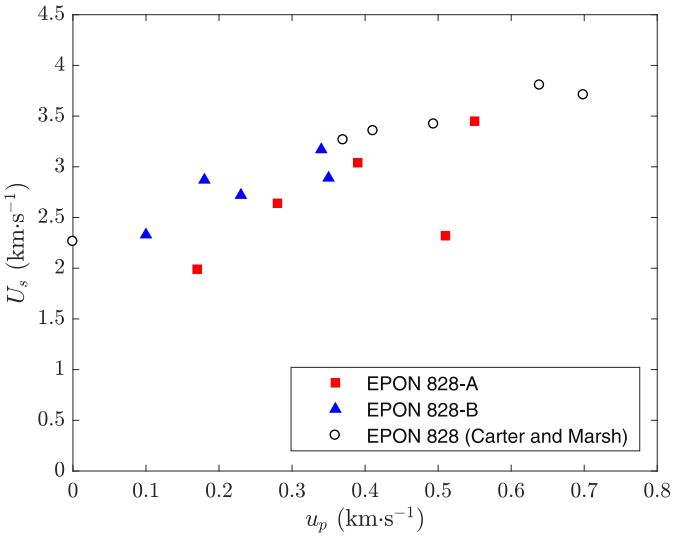

Fig. 8. U_s–u_p measurements for both EPON 828 variants plotted with data by Carter and Marsh for comparison [18].

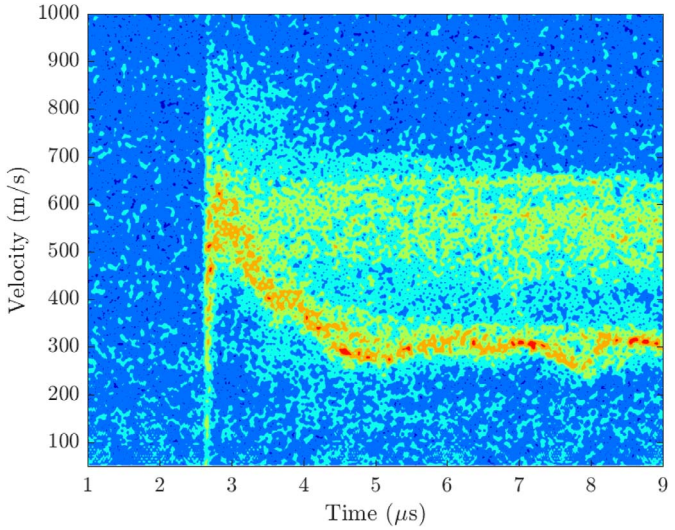

Fig. 9. An unpolished EPON 828-A target impacted with a 6061-T6 aluminum flyer plate at a velocity of 363 m · s^{-1}.

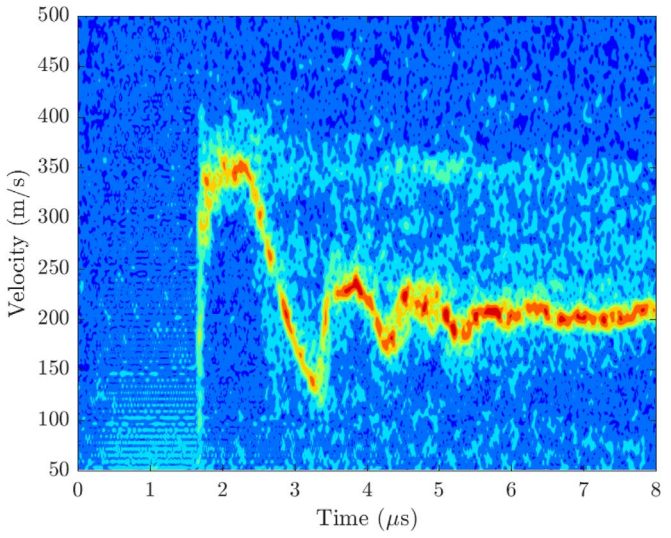

Fig. 10. A polished EPON 828-B target impacted with a PMMA flyer plate at a velocity of 344 m · s^{-1}.

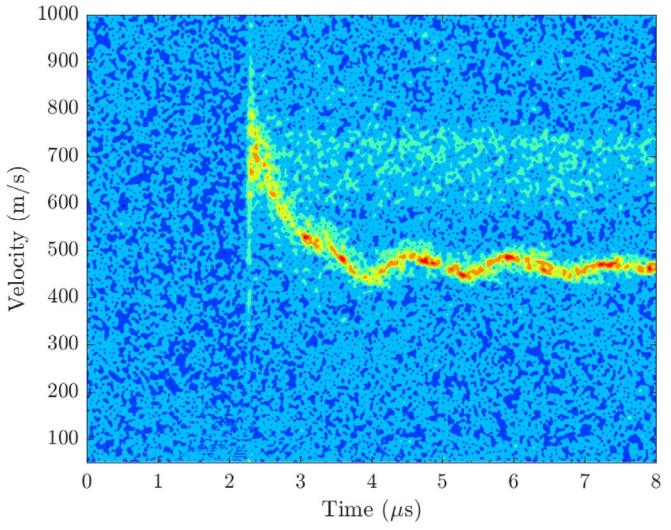

Fig. 11. A polished EPON 828-B target impacted with a 6061-T6 aluminum flyer plate at a velocity of 471 m · s^{-1}.

agent had little or no effect on the shock response of the epoxy system. This is consistent with the work of Munson and May [27], where it was shown that variations in the molecular structure of the polymer chains (caused by changing the curing agent) had no effect on the high-pressure compression response of the resulting epoxy systems. They deduced from their results that the curing agents had no appreciable effect on the equilibrium positions of the backbone chains. Similar reasoning can be used to explain the results of the present study. From Eq. (4), one can use the U_s–u_p relationship to comparatively discuss material compressibility, so the results can be interpreted as confirming a lack of variation in the equilibrium spacing of adjacent backbone chains between EPON 828-A and EPON 828-B.

The present measurements of spall strength and fracture toughness in PMMA are in agreement with the strain-independent values reported in the literature [29,36]. This material was used as a verification of the experimental and analytical methods used in the present study, particularly the choice of pullback velocity from the spectrograms. From Fig. 12, the spall strengths measured in both EPON 828-A and EPON 828-B were found to be considerably higher than those of PMMA. These results also demonstrate that the spall strengths of the epoxies are strongly dependent on the curing agent. In Fig. 13, the results show a strain-rate dependence of the spall strengths for both epoxies, which again differ from the response of PMMA. The spall strength of EPON 828 has been previously reported to be 76 MPa [30,56], which is remarkably lower than the average value of 444 MPa reported in the present study.

There are a few possible explanations for this discrepancy between the results of the present study and those of reported by Guess in 1968 [30]. The strong influence of the curing agent on the spall strength is evident from Figs. 12 and 13, where the spall strength of EPON 828-A was, on average, approximately 29% higher than that of EPON 828-B. Such a considerable difference between contemporary curing agents for a resin system, which have been optimized throughout years of research may explain the even larger variation between studies resulting from the choice of curing agent for the epoxy. An alternative explanation is the influence of the flyer plate material choice on the interpretation of the spall signal.

The choice of flyer plate material will also influence the back face velocity profile, which can lead to the misidentification of the pullback velocity (u_{pull}). The common approach to spall testing involves impacting the specimen with a thin metallic flyer plate. When the test material is a metal, the backface velocity signal is often identical to the

Table 2
The quantitative results of the plate impact experiments.

Shot #	Target	w_t (mm)	Flyer Plate	v_i ($m \cdot s^{-1}$)	σ_{sp} (MPa)	ϵ_r (s^{-1})	K_c ($MPa \cdot m^{1/2}$)	u_p ($km \cdot s^{-1}$)	U_s ($km \cdot s^{-1}$)	σ_H (GPa)	ϵ_H
1	PMMA	6.55	PMMA	203	164	3.8×10^4	3.5	0.10	2.98[a]	0.34[a]	0.03[a]
2	PMMA	6.55	PMMA	252	164	3.4×10^4	3.8	0.11	3.00[a]	0.38[a]	0.04[a]
3	PMMA	6.60	PMMA	357	158	1.0×10^5	2.0	0.18	3.12[a]	0.67[a]	0.06[a]
4	PMMA	6.50	PMMA	498	158	3.4×10^4	3.5	0.25	3.20[a]	0.95[a]	0.08[a]
5	PMMA	6.53	PMMA	563	160	5.5×10^4	2.8	0.28	3.22[a]	1.07[a]	0.09[a]
6	PMMA	6.55	6061-T6	208	153	8.0×10^4	2.2	0.16	1.97	0.38	0.08
7	PMMA	6.53	6061-T6	502	180	6.0×10^4	3.3	0.35	3.24	1.36	0.11
8	PMMA	8.26	6061-T6	606	168	5.1×10^4	3.2	0.39	3.28[a]	1.51[a]	0.12[a]
9	PMMA	8.45	6061-T6	656	199	1.6×10^5	2.3	0.41	3.29[a]	1.59[a]	0.12[a]
10	PMMA	6.55	6061-T6	722	182	7.4×10^4	3.0	0.51	3.04	1.83	0.17
11	EPON 828-A	5.44	PMMA	136	N.S.[b]	–	–	–	–	–	–
12	EPON 828-A	6.50	6061-T6	219	404	3.2×10^4	14.8	0.17	1.99[d]	0.41	0.09
13	EPON 828-A	5.38	6061-T6	363	445	4.0×10^4	15.3	0.28	2.64	0.88	0.11
14	EPON 828-A	6.58	6061-T6	503	525	4.5×10^4	18.4	0.39	3.04	1.39	0.13
15	EPON 828-A	6.43	6061-T6	671	571	5.5×10^4	19.0	0.51	2.32[d]	1.41	0.22
16	EPON 828-A	6.27	6061-T6	715	585	7.6×10^4	16.7	0.55	3.45	2.27	0.16
17	EPON 828-B	6.68	PMMA	344	339	5.2×10^4	9.0	0.18	2.87	0.60	0.06
18	EPON 828-B	6.53	PMMA	638	392	7.0×10^4	9.6	0.34	3.17[c]	1.29[c]	0.11[c]
19	EPON 828-B	6.58	6061-T6	118	N.S.[b]	–	–	0.10	2.33	0.27	0.04
20	EPON 828-B	6.58	6061-T6	318	339	3.1×10^4	11.6	0.23	2.72	0.72	0.08
21	EPON 828-B	6.60	6061-T6	471	397	5.6×10^4	10.9	0.35	2.89	1.19	0.12

[a] Shock transit times were not measured in shots 1–5, 8, and 9. Instead, U_s was calculated using the empirical polynomial $U_s = 6.486u_p^3 - 7.823u_p^2 + 3.549u_p + 2.703$ provided by Jordan et al. for $u_p \leq 0.4\,km \cdot s^{-1}$ [17].

[b] The term N.S. refers to a no-spall shot, where the characteristic velocity pullback signal was not observed on the velocity profile.

[c] Shock transit times were not measured in shot 18. Instead, U_s was calculated using the empirical polynomial $U_s = 0.848u_p^3 - 2.221u_p^2 + 3.287u_p + 2.275$, a polynomial fitted to experimental data by Carter and Marsh for $u_p \leq 1.0\,km \cdot s^{-1}$ [18].

[d] Non-planar flyer plate impact appears to have affected the shock transit time measurements for shots 12 and 15, based on our spotting laser measurements, causing error in the associated shock velocities.

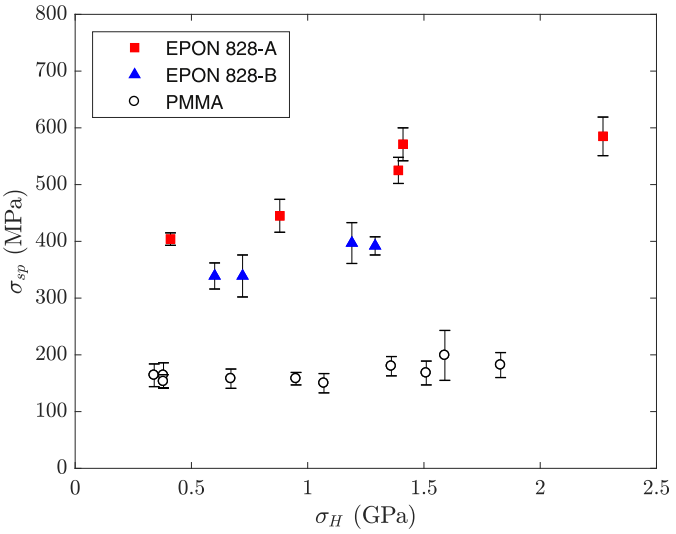

Fig. 12. Strength measurements for EPON 828-A, EPON 828-B, and PMMA plotted against Hugoniot state stress.

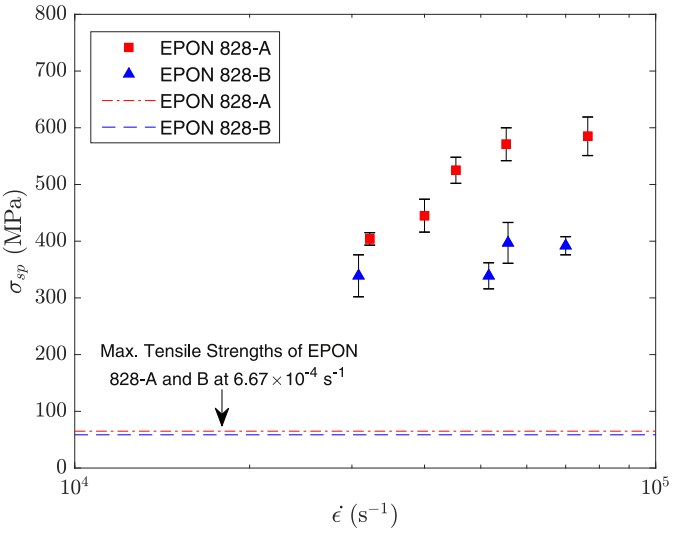

Fig. 13. Strength measurements for EPON 828-A and EPON 828-B at low (quasi-static) and high (shock) strain rates.

idealized velocity profile shown in Fig. 6, with a sharp increase in the velocity to signal the spall event. The backface velocity profiles of spall tests with polymers often feature only a slight velocity increase following a spall event, which is seen in Fig. 9.

Note that in Figs. 9 and 11 slight velocity plateaus are seen in the release signal from the test material. In Fig. 9, this feature is seen at 3.5 μs and a velocity near 400 $m \cdot s^{-1}$, while it is seen at 3 μs and 520 $m \cdot s^{-1}$ in Fig. 11. These features are only seen for an aluminum flyer and are not present in the release velocity profile in tests with the PMMA flyer plate (Fig. 10), resulting in a less ambiguous spall signal. An analysis of the wave dynamics within the test system will show that the plateaus seen for the aluminum flyer tests are the result of the finite thickness of a flyer plate with an impedance that is significantly higher than the test material and are not indicative of the spall event. The first minimum in backface velocity, rather than a plateau, was taken for the spall strength estimate. Using two different flyer plates at similar impact velocities (see shot 17 and shot 20 in Table 2) shows that this approach results in consistent measurements. Choosing the plateau velocity from tests with aluminum flyer plates resulted in spall strengths that were much closer, but still greater than the strength published by Guess [30], however the results were inconsistent with PMMA flyer plate tests. The effect of the flyer plate material on the interpretation of spall signals is a possible cause of the discrepancies between the values reported in the present study and those published previously [30].

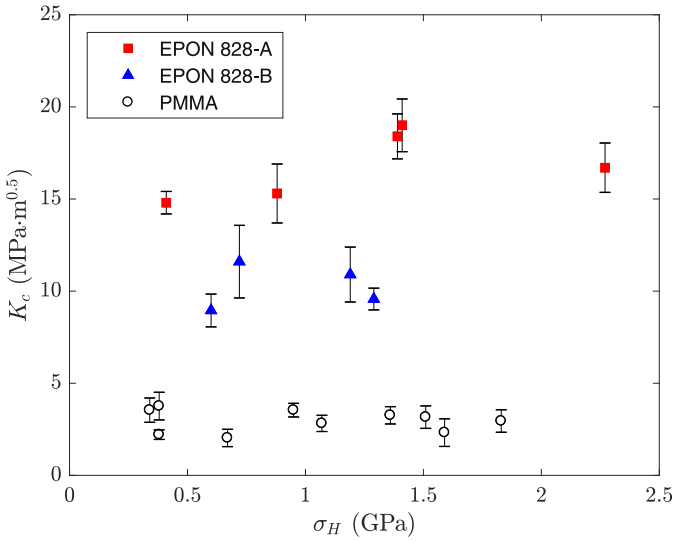

Fig. 14. Fracture toughness measurements for EPON 828-A, EPON 828-B, and PMMA plotted against Hugoniot state stress.

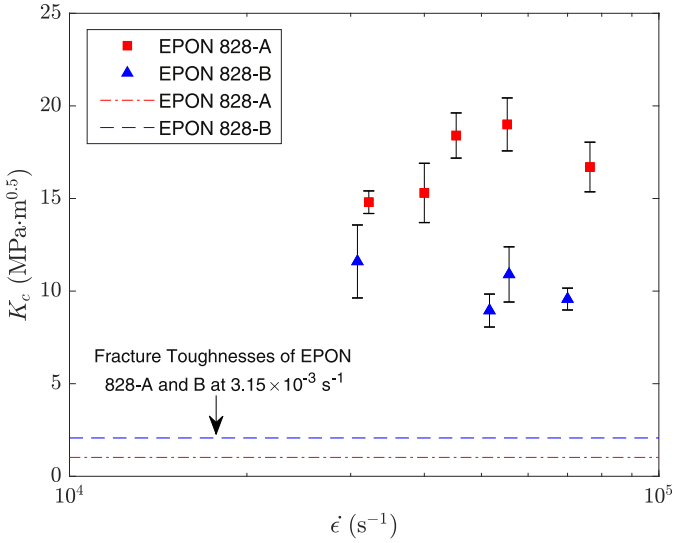

Fig. 15. Fracture toughness measurements for EPON 828-A and EPON 828-B at low (quasi-static) and high (shock) strain rates.

5.1. Strain rate effects

A significant difference between the quasi-static and dynamic mechanical properties of EPON 828-A and EPON 828-B can be observed in Figs. 13 and 15, where values of tensile strength and fracture toughness increase by approximately one order of magnitude between the low and high strain rate domains. The same response is seen for PMMA, albeit to a lesser extent. Interestingly, while the quasi-static tensile strength of PMMA is slightly higher than that of either EPON 828 variant (Table 1), the opposite is seen among the spall strengths of the materials, where the EPON 828 variants have higher dynamic tensile strengths. A pronounced strain rate dependency is also observed in the fracture toughness measurements, where the epoxies are significantly tougher than PMMA at high strain rates, but perform similarly to it under quasi-static loading conditions.

Pronounced microstructure-dependent strain rate effects are well-documented for thermoplastic and thermosetting polymers [36,57–59]. The Ree-Eyring theory [60] is quite applicable here, which is an analytical model that describes the flow of a material as being controlled by the simultaneous interactions of multiple rate-activated processes. When applying this theory to plasticity in polymers, these processes are assumed to be related to specific degrees of freedom of the backbone chains. From this, the transition in yield behaviour observed from quasi-static to dynamic loading conditions is explained in terms of molecular mobility. Resistance to material deformation in the context of a high strain rate deformation of a polymer has been attributed to the restriction of the degrees of freedom within a polymer chain [36]. Thus, the strengthening and toughening effects observed in EPON 828-A, EPON 828-B, and PMMA can be attributed to the restriction of the mobility of the individual molecular chains at high strain rate. A similar effect is seen in dense particle suspensions under high-strain-rate loading, where the sudden jamming of their structure results in a significant increase in stiffness [54,61].

5.2. Effect of shock pressure

The aforementioned strain rate effect is clearly present in these polymers when comparing the quasi-static maximum tensile strengths to the spall strengths. The correlation between spall strength and tensile strain rate (Fig. 13) shows a similar response, where spall strength is strongly strain-rate dependent; however, this strain rate data is not independent of increasing shock pressure. From Fig. 12, the spall strength is shown to be similarly dependent on the shock pressure of the loading wave. A comparison of the results from shot 17 and shot 21 in Table 2 suggests that the spall strength in EPON 828-B is more strongly dependent on the incident shock pressure, as opposed to the strain rate of unloading. This comparison was achieved through the use of flyer plates of different materials, which enabled us to vary shock pressure. The strain rates of these two experiments were $5.2 \cdot 10^4$ s^{-1} and $5.6 \cdot 10^4$ s^{-1}, with corresponding pressures of 0.60 GPa and 1.19 GPa, resulting in spall strengths of 339 MPa and 397 MPa, respectively. This suggests that the shock pressure is dominant in the spall response of these materials, however, the data is too limited to draw definite conclusions.

5.3. Effect of curing agent

The results of the present study clearly demonstrates that the choice of curing agent has a direct effect on the quasi-static and dynamic mechanical properties of the resultant epoxy, despite its negligible influence on shock wave propagation. Among the EPON 828 variants, EPON 828-A has consistently higher tensile strength than EPON 828-B at any given strain rate. In terms of fracture toughness, the results are more complex. While EPON 828-B has a higher fracture toughness than EPON 828-A under quasi-static loading conditions, the opposite trend is seen for fracture toughness, with EPON 828-A exhibiting a larger fracture toughness under dynamic loading.

The distinguishing features of these two curing agents may provide an explanation of this behaviour. Millett et al. [23] demonstrated that variation in the atoms attached to the polymer backbone in thermoplastics can change their macroscopic dynamic behaviour. Functionalizing the backbone chains via the introduction of a curing agent to encourage crosslinking, reduction of free volume, or reduction of the characteristic spacing could potentially result in a variation in the binding forces experienced between adjacent backbone chains. Variation in the binding forces would likely translate to differences in macroscopic mechanical properties, including spall strength and fracture toughness. This provides a possible explanation for the observed behaviour, where one curing agent may promote more or less crosslinking between backbone chains than another, which would result in variation in the dynamic mechanical properties between the different epoxy systems. Following this explanation leads to the likely conclusion that EPON 828-A has greater crosslinking between adjacent polymer chains than EPON 828-B.

6. Conclusions

The objective of this study was to investigate the effect of the curing agent on the dynamic tensile failure behaviour and shock response of an epoxy system. This was achieved by comparing the maximum tensile strength and fracture toughness of the systems measured under both quasi-static and dynamic loading conditions. The choice of curing agent was shown to have a significant effect of the spall strength and fracture toughness of the epoxy resin, but no appreciable effect on shock response, as seen from the shock Hugoniot. Spall strength measurements ranged from 404 to 585 MPa in EPON 828-A and from 339 to 397 MPa in EPON 828-B at strain rates on the order of 10^4 s^{-1}. Fracture toughness measurements ranged from 14.8 to 19.0 $MPa \cdot m^{½}$ in EPON 828-A and from 8.95 to 11.6 $MPa \cdot m^{½}$ in EPON 828-B at strain rates on the order of 10^4 s^{-1}. These results were attributed to the micromechanical behaviour observed between adjacent polymer chains, whereby the binding forces and equilibrium spacing were speculated to present the largest contribution to the failure behaviour.

Acknowledgements

The authors would like to thank Andrew Higgins for granting access to his research facility. Financial support by the National Research Council Canada (NRC) through the Security Materials Technology (SMT) program is also appreciated.

References

[1] Kinloch AJ, Mohammed RD, Taylor AC, Eger C, Sprenger S, Egan D. The effect of silica nano particles and rubber particles on the toughness of multiphase thermosetting epoxy polymers. J Mater Sci 2005;40(18):5083–6.
[2] Wu L, Hoa SV, Ton-That M-T. Effects of composition of hardener on the curing and aging for an epoxy resin system. J Appl Polym Sci 2006;99(2):580–8.
[3] Razack NA, Varghese LA. The effect of various hardeners on the mechanical and thermal properties of epoxy resin. Int J Eng Reseach Technol 2014;3(1):2662–5.
[4] Stout MG, Koss DA, Liu C, Idasetima J. Damage development in carbon/epoxy laminates under quasi-static and dynamic loading. Compos Sci Technol 1999;59(16):2339–50.
[5] Dandekar DP, Hall CA, Chhabildas LC, Reinhart WD. Shock response of a glass-fiber-reinforced polymer composite. Compos Struct 2003;61(1-2):51–9.
[6] Zaretsky E, DeBotton G, Perl M. The response of a glass fibers reinforced epoxy composite to an impact loading. Int J Solids Struct 2004;41(2):569–84.
[7] Setchell RE, Anderson MU. Shock-compression response of an alumina-filled epoxy. J Appl Phys 2005;97(8):083518.
[8] Yuan F, Tsai L, Prakash V, Rajendran AM, Dandekar DP. Spall strength of glass fiber reinforced polymer composites. Int J Solids Struct 2007;44(24):7731–47.
[9] Lopes PE, Hattum FV, Pereira C, Nóvoa P, Forero S, Hepp F, et al. High CNT content composites with CNT buckypaper and epoxy resin matrix: impregnation behaviour composite production and characterization. Compos Struct 2010;92(6):1291–8.
[10] Pol MH, Liaghat G. Investigation of the high velocity impact behavior of nanocomposites. Polym Compos 2016;37(4):1173–9.
[11] Hoffman DM. Dynamic mechanical signatures of Viton A and plastic bonded explosives based on this polymer. Polym Eng Sci 2003;43(1):139–56.
[12] Milne A, Longbottom A, Bourne NK, Millett JCF. On the unreacted hugoniots of three plastic bonded explosives. Propellants, Explos Pyrotech 2007;32(1):68–72.
[13] Grujicic M, Bell WC, Pandurangan B. Design and material selection guidelines and strategies for transparent armor systems. Mater Des 2012;34:808–19.
[14] Hazell PJ. Armour: materials, theory, and design. ed.: 1st Boca Raton: CRC Press; 2015.
[15] Patel PJ, Hsieh AJ, Gilde GA. Improved low-cost multi-hit transparent armor. Tech. Rep.. Aberdeen Proving Ground: U. S. Army Research Laboratory; 2006.
[16] Barker LM, Hollenbach RE. Shockwave studies of PMMA, fused silica , and sapphire. J Appl Phys 1970;41(10):4208–26.
[17] Jordan JL, Casem D, Zellner M. Shock response of polymethylmethacrylate. J Dyn Behav Mater 2016;2(3):372–8.
[18] Carter WJ, Marsh SP. Hugoniot equation of state of polymers. Tech. Rep.. Los Alamos: Los Alamos National Laboratory; 1995.
[19] Fu Y, Michopoulos J, Song J-H. Dynamics response of polyethylene polymer nanocomposites to shock wave loading. J Polym Sci Part B Polym Phys 2015;53(18):1292–302.
[20] Chen W, Lu F, Cheng M. Tension and compression tests of two polymers under quasi-static and dynamic loading. Polym Test 2002;21(2):113–21.
[21] Curran DR, Shockey DA, Seaman L. Dynamic fracture criteria for a polycarbonate. J Appl Phys 1973;44(9):4025–38.
[22] Faye A, Parmeswaran V, Basu S. Mechanics of dynamic fracture in polycarbonate. Procedia Mater Sci 2014;3:1304–9.
[23] Millett JCF, Brown EN, Gray GT, Bourne NK, Wood DC, Appleby-Thomas G. The effects of changing chemistry on the shock response of basic polymers. J Dyn Behav Mater 2016;2(3):326–36.
[24] Millett JCF, Bourne NK, Barnes NR. The behavior of an epoxy resin under one-dimensional shock loading. J Appl Phys 2002;92(11):6590–4.
[25] Millett JCF, Bourne NK. The deviatoric response of polymethylmethacrylate to one-dimensional shock loading. J Appl Phys 2000;88(12):7037–40.
[26] Jain R, Kukreja P, Narula AK, Chaudhary V. Studies of the curing kinetics and thermal stability of epoxy resins using a mixture of amines and anhydrides. J Appl Polym Sci 2006;100(5):3919–25.
[27] Munson DE, May RP. Dynamically determined high-pressure compressibilities of three epoxy resin systems. J Appl Phys 1972;43(3):962–71.
[28] Golubev VK, Novikov SA, Sobolev YS. Effect of temperature on spall of polymer materials. J Appl Mech Tech Phys 1982;23(1):134–41.
[29] Parhomenko IP, Utkin AV. Matter under extreme conditions. Moscow: IVTAN; 1990.
[30] Guess TR. Some dynamic mechanical properties of an epoxy. Tech. Rep. SC-DR-68-343. Albuquerque: Sandia Laboratories; 1968.
[31] Epon resin 828. Tech. Rep.. Hexion Inc.; 2005.
[32] Epikure curing agent 3200, 3223, 3234 & 3245. Tech. Rep.. Hexion Inc.; 2005.
[33] Epikure curing agent 3233. Tech. Rep.. Hexion Inc.; 2007.
[34] Glemco Inc.. 6061-T6 aluminum. Tech. Rep.. Glemco Inc.; 2016.
[35] Arkema Inc.. Plexiglas G. Tech. Rep.. Arkema Inc.; 2013.
[36] Weerasooriya T, Moy P, Casem D, Chen W. Fracture toughness for PMMA as a function of loading rate. SEM Annu. Conf. Expo. Exp. Appl. Mech. St. Louis. 2006.
[37] Strand OT, Goosman DR, Martinez C, Whitworth TL. Compact system for high-speed velocimetry using heterodyne techniques. Rev Sci Instrum 2006;77(8):083108.
[38] Cooper PW. Explosives engineering. ed.: 4th New York: Wiley-VCH; 2002.
[39] Antoun T, Seaman L, Curran DR, Kanel GI, Razorenov SV, Utkin AV. Spall fracture. ed.: 1st New York: Springer-Verlag; 2003.
[40] Kanel GI, Razorenov SV, Fortov VE. Shock-wave phenomena and the properties of condensed matter. ed.: 1st New York: Springer Science & Business Media; 2004.
[41] Meyers MA, Aimone CT. Dynamic fracture (spalling) of metals. Prog Mater Sci 1983;28(1):1–96.
[42] Chevrier P, Klepaczko JR. Spall fracture: mechanical and microstructural aspects. Eng Fract Mech 1999;63(3):273–94.
[43] Kanel GI. Spall fracture: methodological aspects, mechanisms and governing factors. Int J Fract 2010;163(1):173–91.
[44] Rice M, McQueen R, Walsh J. Compression of solids by strong shock waves. Solid State Phys 1958;6:1–63.
[45] Meyers MA. Dynamic behavior of materials. ed.: 1st New York: Wiley-InterScience; 1992.
[46] Novikov SA, Divinov II, Ivanov AG. Failure of steel, aluminum and copper under explosive shock loading. Phys Met-Metallogr 1966;21(4):122–8.
[47] Stepanov GV. Spall fracture of metals by elastic-plastic loading waves. Probl Prochnosti 1976;8:66–70.
[48] Luo SN, An Q, Germann TC, Han LB. Shock-induced spall in solid and liquid Cu at extreme strain rates. J Appl Phys 2009;106(1):013502.
[49] Grady DE. The spall strength of condensed matter. J Mech Phys Solids 1988;36(3):353–84.
[50] Kinloch AJ, Shaw SJ, Tod DA, Hunston DL. Deformation and fracture behaviour of a rubber-toughened epoxy: 1. Microstructure and fracture studies. Polymer (Guildf) 1983;24(10):1341–54.
[51] Xia Y, Wang X, Yang B. Brittle-ductile-brittle transition of glass fibre-reinforced epoxy under tensile impact. J Mater Sci Lett 1993;12(18):1481–4.
[52] Wei W, Guowei M. Failure mechanism of epoxy polymer: transition from ductile to brittle failure. Fourth Int. Conf. Exp. Mech.. 7522. S1ingapore; 2009. p. 75225L–1.
[53] Barker LM, Hollenbach RE. Laser interferometer for measuring high velocities of any reflecting surface. J Appl Phys 1972;43(11):4669–75.
[54] Petel OE, Higgins AJ. Shock wave propagation in dense particle suspensions. J Appl Phys 2010;108(11):114918.
[55] Prudhomme G, Mercier P, Berthe L. PDV experiments on shock-loaded particles. J. Phys. Conf. Ser.. 500. Seattle; 2014. 142027
[56] Lundergan CD, Drumheller DS. Propagation of stress waves in a laminated plate composite. J Appl Phys 1971;42(2):669–75.
[57] Richeton J, Ahzi S, Jiang FC, Adharapurapu RR. Influence of temperature and strain rate on the mechanical behavior of three amorphous polymers: characterization and modeling of the compressive yield stress. Int J Solids Struct 2006;43(7-8):2318–35.
[58] Mulliken AD, Boyce MC. Mechanics of the rate-dependent elastic plastic deformation of glassy polymers from low to high strain rates. Int J Solids Struct 2006;43(5):1331–56.
[59] Bie BX, Han J-H, Lu L, Zhou XM, Qi ML, Zhang Z, et al. Dynamic fracture of carbon nanotube/epoxy composites under high strain-rate loading. Compos Part A Appl Sci Manuf 2015;68:282–8.
[60] Ree T, Eyring H. Theory of non-Newtonian flow. I. Solid plastic system. J Appl Phys 1955;26(7):793–800.
[61] Petel OE, Frost DL, Higgins AJ, Ouellet S. Shock-induced formation of a disordered solid from a dense particle suspension. Phys Rev E 2012;85(2):021401.